Ann. Geophys., 25, 1391–1403, 2007
www.ann-geophys.net/25/1391/2007/

Annales Geophysicae

Eigenmode analysis of ballooning perturbations in the inner magnetosphere of the Earth

A. S. Parnowski

Space Research Institute NASU-NSAU, Kyiv, Ukraine

Received: 4 January 2007 – Revised: 10 April 2007 – Accepted: 31 May 2007 – Published: 29 June 2007

Abstract. We analyze coupled Alfvén and slow magnetosonic eigenmodes in a dipole geomagnetic field with different ionospheric conductivities in the framework of ideal magnetic hydrodynamics (MHD) with finite pressure. We use numerical and, if possible, analytical methods to describe eigenmode frequencies, growth rates and eigenfunctions. The spectrum of Alfvén and slow magnetosonic modes is discrete and equidistant. The frequencies of the first Alfvén and slow magnetosonic eigenmodes are estimated as $\sim$1 Hz and $\sim$1 mHz, respectively. In the case of finite conductivity, periodic and aperiodic modes are separated and their interaction analyzed. It was shown that periodic and aperiodic perturbations can mutually transform into each other. A new flute stability criterion is derived ($\alpha\sim$4.25), which is stricter than the Gold criterion (α=20/3). Here, as usual, $\alpha=-L/p\,dp/dL$. For flute perturbations, the deviations of transversal displacement from a constant are calculated. An approximation for longitudinal displacement is derived. We determined the position of the main longitudinal peak, which can be responsible for nonlinear structures observed by Freja. An influence of nonlinear terms in pressure is estimated as well.

Keywords. Magnetospheric physics (Magnetosphere-ionosphere interactions; MHD waves and instabilities)

1 Introduction

This article is dedicated to the analysis of the eigenmode spectrum of transversally small-scale ULF MHD perturbations in the inner magnetosphere of the Earth. This analysis is an important part of the investigation of waves and instabilities in the magnetospheric plasma. This investigation, in turn, is important for understanding the processes which accompany the substorm onset (particularly, Pi1 and Pi2 pulsations, which fall in the same frequency band as the considered processes). Such research can eventually lead to the creation of "space weather" models.

Plasma confined by the geomagnetic field is in a thermodynamical non-equilibrium like any other plasma with pressure. Therefore, according to general theory of plasma instabilities, it can spontaneously acquire collective degrees of freedom, thus becoming unstable. Magnetospheric plasma never occupies a low-energy state, due to the constant flow of energy from outside. In trying to reach the minimum energy state, the magnetosphere constantly generates unstable perturbations, which change its configuration and transport properties.

Some instabilities are associated with motions of macroscopic volumes of plasma and can be described with MHD equations. The other instabilities, which essentially depend on the difference in motions of different groups of particles in the same volume, are called kinetic instabilities. They are microscopic in comparison to large-scale slow MHD motions. The greatest threat to plasma stability is posed by MHD instabilities with large growth rates, which lead to a rapid reconstruction of the initial equilibrium. As magnetospheric plasma pressure grows, the main role goes to MHD instabilities, which are powered by plasma's thermal energy. These are flute and ballooning modes, which are driven by pressure and magnetic field line curvature.

The first stability criterion for flute modes was intuitively obtained in a pioneering paper (Gold, 1959) in the form α/γ=4. The designations will be explained below. Note that this criterion is analogous to the convective stability condition of gas, compressed by a gravity field. Although being the main interchange criterion for a long time, the Gold criterion became a very controversial subject, enlisting both supporters and opponents. A very similar criterion was obtained by Southwood and Kivelson (1989), who dealt with finite pressure plasma. However, the Gold criterion was criticized by Cheng (1985), who disputed the integrability of the

Correspondence to: A. S. Parnowski
(dyx@ikd.kiev.ua)

Published by Copernicus Publications on behalf of the European Geosciences Union.

energetic principle along the field lines, which would lead to a completely different criterion. This statement was later supported by Liu (1996), who also criticized the confirmation of the Gold criterion by Rogers and Sonnerup (1986), stating that it was only due to an incidental property of the toroidal model used. We tend to agree with Liu (1996), because, as it was shown by Chan et al. (1994), the dipole flux surface is pushed outward by the finite pressure and taking this effect into account would lead, in our opinion, to a significant distortion of the stability criterion. This statement is additionally proven by this article, as it shows that in the case of curved magnetic field lines, the transversal amplitude of flute perturbations deviates from the constant and is accompanied by significant longitudinal displacements. The stability criterion derived in the paper by Cheremnykh and Parnowski (2006a) and later improved in the paper by Cheremnykh and Parnowski (2006b) is by about one-third less than the Gold criterion ($\sim$4.25 against $\sim$6.67). Given the problem that radial pressure gradients in the magnetosphere (Lui and Hamilton, 1992; DeMichelis et al., 1999) are insufficient to break the Gold criterion, it is crucial to determine which instabilities can be triggered in the magnetosphere. Besides, interchange instability can explain the strong ejections of plasma at the time of magnetospheric substorms (Swift, 1967).

Ballooning modes are well known in the magnetic fusion literature as pressure driven instabilities, analogous to the instability developing at a weak spot of a pressurized elastic container. Ballooning perturbations are also sometimes called transversally small-scale modes. The assumption of smallness of the transversal scale of perturbations has a profound physical meaning: (fast) magnetosonic waves, exhibiting themselves in compression and depression of field lines and being suppressed by the stationary magnetic field of the Earth at low plasma pressure, are thrown away and only Alfvén and slow magnetosonic (acoustic) waves, which are the most dangerous to the stability, are considered. So, perturbations of plasma, submersed in a stationary magnetic field, are a hybrid of Alfvén and slow magnetosonic waves. It is just these waves which form perturbations of the ballooning type. In the case of the magnetosphere, such a stationary field is the geomagnetic one, and in the case of fusion research, the stationary field of a device. This is one of the reasons why ballooning modes are so important in magnetospheric and fusion research.

This article is a further development of our earlier research (Cheremnykh and Parnowski, 2004, 2006b), (Cheremnykh et al., 2004). We omit the derivation of the equations for the sake of brevity; those interested should consult either Cheremnykh et al. (2004) or, preferably, Cheremnykh and Parnowski (2006b). We would, however, indicate that this derivation was identical in the sense that we did not use any nonidentical operators, except for the ballooning approximation, so we believe that the eigenmode spectrum of our equations coincides with that of the original MHD equations for ballooning perturbations.

The set of equations describing Alfvén, slow and fast magnetosonic waves, which took into account finite ionospheric conductivity, was identically obtained from the MHD equations by Klimushkin (1997). However, he used a box model of the magnetosphere and therefore missed an important phenomenon of Alfvén-magnetosonic coupling. He associated the eigenmodes of the Alfvén resonator with Pc4 pulsations. This was also pointed out by Mager and Klimushkin (2002), who found out that Pc4 pulsations cannot exist in the absence of plasma pressure due to the transparency region being too narrow in this case. They came to the conclusion that magnetospheric MHD waves should be investigated only when a field line curvature and plasma pressure are taken into account.

Lakhina et al. (1990) took into account the influence of plasma co-rotation as a toroidal mass flow with an arbitrary Mach number on arbitrary polarized ballooning perturbations of plasma with arbitrary pressure. They managed to obtain the equilibrium equation for this case. Using the energetic principle, they obtained that toroidal flow does not generate ballooning modes, but rather stabilizes or destabilizes a present stable or unstable situation. Thus, plasma co-rotation does not affect stability.

Hameiri et al. (1991) also considered the gravitational potential; however, they switched to the cold pressureless plasma limit when calculating the ballooning frequencies.

Thus, the model used in this article, unlike others, takes into account magnetic field line curvature, plasma pressure, boundary conductivity and arbitrary polarization of perturbations simultaneously.

2 The equations of small oscillations

We identically derived the equations of small oscillations from ideal MHD equations using the definition of the magnetic label and the static plasma equilibrium $\nabla p = [\boldsymbol{j}\boldsymbol{B}]$, provided by a dipole magnetic field $\boldsymbol{B}$ and a toroidal current $\boldsymbol{j}$, in terms of a plasma displacement vector $\boldsymbol{\xi}$. Isotropic pressure was assumed. We also neglected the convection and the deviations from the dipole field due to the low-beta approximation used. Applying ballooning approximation to them, we obtain the Dewar and Glasser (1983) equations describing ballooning perturbations in an arbitrary geometry of the magnetic field. Then we cast the dipole magnetic field into them and rewrite them for an individual magnetic field line, taking into account that ballooning perturbations are field-line-driven. After that, we rewrote them in a dimensionless form (Cheremnykh and Parnowski, 2006b)

$$\Omega^2 c^6 b^{-1}\xi\left(1+\lambda^2 b\right)+4c^4 b^{-2}\left(T_0+\alpha\beta\gamma^{-1}\xi\right) + \left[\left(1+\lambda^2 b\right)b^{-1}\xi'\right]'=0, \quad (1)$$

$$\eta+\lambda\xi=0, \quad (2)$$

$$\Omega^2\tau + c^{-3}T_0' = 0, \quad (3)$$

$$T_0 = \left(\beta^{-1} + c^6 b^{-1}\right)^{-1}\left[c^{-3}\left(c^6 b^{-1}\tau\right)' - 4cb^{-2}\xi\right], \quad (4)$$

where the prime indicates a derivative with respect to $x=\sin\theta$ along the field line, $b=1+3x^2$, and $c=1-x^2$. The coordinate system is spherical (φ is the toroidal angle (geomagnetic longitude), θ is the poloidal angle (geomagnetic latitude), and $r=L\cos^2\theta$ is the equation for the geocentric radius of the field line) for the parameters and Cartesian ($\frac{\boldsymbol{B}}{|\boldsymbol{B}|^2}$ – longitudinal, $\frac{\nabla\psi}{|\nabla\psi|^2}$ – poloidal, $\frac{[\boldsymbol{B}\nabla\psi]}{|\boldsymbol{B}|^2}$ – toroidal) for the displacement components. The term "poloidal displacement" is used here in the same sense as in the article by Hameiri et al. (1991), i.e. a displacement in a direction normal to the magnetic surface. Note that when speaking about fields, it is common to call this direction "scaloidal", as proposed by Elsasser (1946). Other quantities in Eqs. (1–4) are: $\Omega=fLc_A^{-1}$ is the dimensionless frequency, f is the actual frequency in Hz, L is the McIlwain (1961) parameter, c_A is the Alfvén velocity, $\boldsymbol{\xi}=\xi\frac{\nabla\psi}{|\nabla\psi|^2}+\eta\frac{[\boldsymbol{B}\nabla\psi]}{|\boldsymbol{B}|^2}+\tau\frac{\boldsymbol{B}}{|\boldsymbol{B}|^2}$ is the plasma displacement vector, $\xi=\boldsymbol{\xi}\nabla\psi$ is the poloidal displacement (Alfvén), $\eta=\boldsymbol{\xi}\frac{[\boldsymbol{B}\nabla\psi]}{|\nabla\psi|^2}$ is the toroidal displacement (Alfvén), $\tau=\boldsymbol{\xi}\boldsymbol{B}$ is the longitudinal displacement (slow magnetosonic), λ is the polarization parameter (Cheremnykh and Parnowski, 2006b; Dewar and Glasser, 1983), $\alpha=-\frac{L}{p}\frac{dp}{dL}$ is the pressure profile, $\beta=\gamma p B_0^{-2}$ is the plasma beta taken on the equatorial plane, $\gamma=5/3$ is the ratio of specific heats, $B_0=ML^{-3}$ is the value of the magnetic field at the equator, M is the magnetic dipole momentum of the Earth, $T_0=\gamma p\mathrm{div}\boldsymbol{\xi}$ is the compressibility of the perturbations, ρ is the mass density of plasma, p is the plasma pressure.

Let us discuss the polarization parameter λ. The ballooning approximation is mathematically equivalent to the application of the transversal eikonal $\exp\left(-ift+i\chi/\varepsilon\right)$, where $\varepsilon\ll 1$ is the characteristic transversal scale, and χ is the eikonal function, which satisfies the condition $\boldsymbol{B}\nabla\chi=0$. The dipole magnetic field can be represented in the form $\boldsymbol{B}=[\nabla\psi\nabla\varphi]$, where $\psi=\frac{M\cos^2\theta}{r}=\frac{M}{L}$ is the magnetic flux. Thus, we can write $[\nabla\psi\nabla\varphi]\nabla\chi=0$, which is equivalent to $\nabla\chi=k_\psi\nabla\psi+k_\varphi\nabla\varphi$, where $k_\psi=\partial\chi/\partial\psi$ and $k_\varphi=\partial\chi/\partial\varphi$ are constant on the field line. The polarization parameter λ, defined as $\lambda=k_\psi/k_\varphi$, is therefore also constant on the field line and is characteristic of the orientation of the $\boldsymbol{k}_\perp=\nabla\chi$ vector, which was identified as a wave vector of the fast magnetosonic wave by Hameiri, Laurence and Mond (1991). For Alfvén waves $\boldsymbol{\xi}_\perp\nabla\chi=\boldsymbol{k}_\perp\boldsymbol{\xi}_\perp=0$, where $\boldsymbol{\xi}_\perp=\boldsymbol{\xi}-\tau\frac{\boldsymbol{B}}{|\boldsymbol{B}|^2}$ is the transversal displacement. Thus, considering Eq. (2), when $\lambda=0$, the perturbations are poloidal ($\boldsymbol{\xi}_\perp=\xi\frac{\nabla\psi}{|\nabla\psi|^2}$), and when $\lambda=\infty$, the perturbations are toroidal ($\boldsymbol{\xi}_\perp=\eta\frac{[\boldsymbol{B}\nabla\psi]}{|\boldsymbol{B}|^2}$). In the case of arbitrary polarization $\boldsymbol{\xi}_\perp=\xi\left(\frac{\nabla\psi}{|\nabla\psi|^2}-\lambda\frac{[\boldsymbol{B}\nabla\psi]}{|\boldsymbol{B}|^2}\right)$.

Equation (1) describes Alfvén modes (transversal), Eq. (2) – their polarization, Eq. (3) – slow magnetosonic modes (longitudinal), Eq. (4) – Alfvén-magnetosonic coupling (plasma compressibility).

Note that in the finite pressure plasma with tied curved magnetic field lines, there are no pure Alfvén or slow magnetosonic modes; both components are always present. We call the eigenmodes "Alfvén" or "slow magnetosonic" after the dominant component. For the Alfvén eigenmode, a longitudinal component is typically several percent of a transversal one, and for a slow magnetosonic eigenmode, it is larger by three to six orders.

The boundary conditions for Eqs. (1–4) in the case of the resistive boundary have the form (Cheremnykh and Parnowski, 2006b)

$$\Omega b\xi\left(1+\lambda^2 b\right) + i\delta \left[2x\left(1+\lambda^2 b\right)\xi' - c^5\left(T_0+\alpha\beta\gamma^{-1}\xi\right)\right]\Big|_{x=\pm x_0} = 0, \quad (5)$$

$$\xi + 2xc\tau|_{x=\pm x_0} = 0, \quad (6)$$

where $\delta=(\Sigma_P c_A)^{-1}$ is the dimensionless squared thickness of the skin layer ($\Sigma_P=\frac{4\pi}{c^2}\Sigma_P^{(\mathrm{CGS})}$, where $\Sigma_P^{(\mathrm{CGS})}$ is the integral Pedersen conductivity of the ionosphere in Gauss units), $x_0=\sqrt{1-L^{-1}}$ is the boundary value of x. Boundary condition (5) states that the magnetospheric current closes on the ionosphere, and Eq. (6) states that the perturbation does not propagate in the atmosphere due to its neutrality and much larger density.

Equations (1–4) can also be obtained from Eqs. (16a, b) from the article by Hameiri (1999), and Eqs. (5), (6) – from Eqs. (17a, b) ibid by substituting $X\to\xi$, $Y\to\frac{c^6}{b}\tau$, $N^2\to c^3\frac{1+\lambda^2 b}{b}$, $B^2\to\frac{b}{c^6}$, $K\to\frac{4c}{b^2}$, $\rho X_{tt}\to-\Omega^2\xi$, $\rho Y_{tt}\to-\frac{c^6}{b}\Omega^2\tau$, $\beta B^2\left(Y'-KX\right)\to T_0$, $\dot{p}\to\frac{\alpha\beta}{\gamma}$, $p\to\frac{\beta}{\gamma}$, $\beta\to\frac{\beta c^6}{b+\beta c^6}$, $N_n\to\frac{c^2}{b}$, $B_n\to\frac{2x}{c^3}$, $\Sigma_\perp\to\frac{2}{\delta^2}$, $()'\to\frac{1}{c^3}()'$. Nevertheless, Eqs. (1–4) were obtained independently from the article by Hameiri (1999), by a different method, and are based on a different model of the magnetosphere. Boundary conditions (5), (6) are identical to those obtained by Hameiri and Kivelson (1991), and later discussed by Hameiri (1999).

Let us consider even and odd linear combinations, such as $\frac{1}{2}(\xi(x)\pm\xi(-x))$. These combinations satisfy Eqs. (1–3) due to their linearity, as well as boundary conditions. Note that even combinations for ξ are connected only with odd combinations for τ and vice versa. We determine the parity of the solution by transversal amplitude (ξ) symmetry; longitudinal amplitude (τ) will have an opposite symmetry. We consider even and odd perturbations separately. Even modes satisfy the additional conditions $\xi'|_{x=0}=0$, $\tau|_{x=0}=0$ and the odd ones – $\xi|_{x=0}=0$, $\tau'|_{x=0}=0$. In general, the solutions of Eqs. (1–3) are a sum of odd and even eigenmodes.

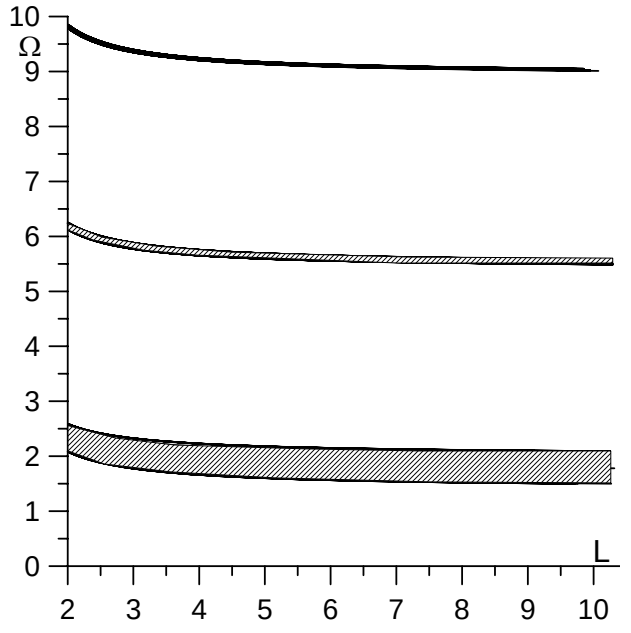

Fig. 1a. Dependence of Alfvén spectrum on McIlwain number in the cold plasma case with ideal conductive ionospheres. The finite width of the spectral lines is due to different eigenmode polarizations (upper limit – toroidal, lower – poloidal).

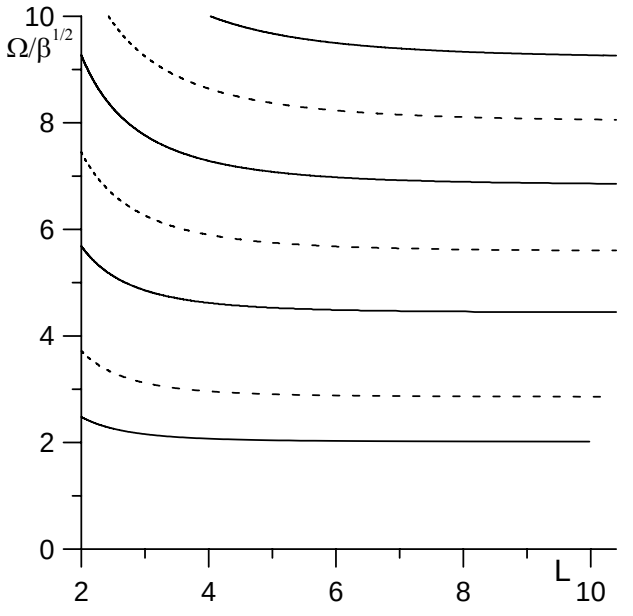

Fig. 1b. The spectrum of slow magnetosonic modes (solids – even, dashes – odd).

3 Conductive boundary

In this case boundary conditions have the form

$$\xi|_{x=\pm x_0} = 0, \quad \tau|_{x=\pm x_0} = 0 \tag{7}$$

and the solutions of Eqs. (1–3) are real. It follows from Eqs. (1), (2) that frequencies of arbitrary polarized perturbations fall between the frequencies of poloidal and toroidal perturbations. Thus, we shall consider primarily these two polarizations.

In the case of toroidal polarization ($\lambda \to \infty$) Eqs. (1), (2) take the form

$$\Omega^2 c^6 \eta + \eta'' = 0, \quad \xi = 0, \tag{8}$$

and Eq. (3) holds. Equation (8) was derived by Cheng et al. (1993). The eigenmode spectrum consists of two independent branches. The first branch is determined by Eq. (8) and the boundary condition (7). Its frequency is determined only by the mode number and McIlwain parameter. The second branch is determined by Eq. (3) and the boundary condition (7). It also depends on plasma beta $\Omega \sim \sqrt{\beta}$. Several lowest modes of each type are presented in Fig. 1a, b, correspondingly in coordinates $(L,\ \Omega)$ and $\left(L,\ \Omega\beta^{-1/2}\right)$. In $\left(\beta,\ \Omega^2\right)$ coordinates the spectrum for fixed L consists of horizontal lines (Alfvén modes) and diagonal lines running through the origin (slow magnetosonic modes). One can see that the eigenmode spectrum is discrete. This suggests that the observed ULF spectrum will also be discrete. Estimated frequencies of slow magnetosonic modes are about 10^{-3} Hz ("low"), and of Alfvén ones – about 10^{-1}–1 Hz ("high").

In the case of poloidal polarization (λ=0) the Eqs. (1), (2) take the form

$$\Omega^2 c^6 b^{-1} \xi + 4c^4 b^{-2} \left(T_0 + \alpha\beta\gamma^{-1}\xi\right) + \left(b^{-1}\xi'\right)' = 0,$$
$$\eta = 0, \tag{9}$$

and Eq. (3) holds. The spectrum is similar to the previous case except for one principal distinction. The intersection points of different branches in the previous case contain degeneration, while in this case this degeneration is lifted due to the presence of perturbing term (4) in Eq. (9). This is seen in the plots as "coupling" of spectral branches (Fig. 2). In these points Alfvén and slow magnetosonic modes mutually transform into each other, and the energy is transferred between "high"- and "low"-frequency oscillations. Near the "coupling" point the eigenmodes cannot be identified as either Alfvén or slow magnetosonic – they are both at once.

The form of these curves can be calculated only numerically. Note that only the spectra of the same parity couple; spectra of different parity intersect and such modes do not interact. For β=0 poloidal frequencies are lower than the toroidal ones (Fig. 1a). The inclination of these lines at low β is determined by α. Figure 2 demonstrates an arbitrary polarized spectrum, confirming that eigenmode frequencies are bounded by poloidal and toroidal frequencies. This plot has an interesting feature: there are three points, β=0.1, 0.2, 0.6, where frequency does not depend on polarization.

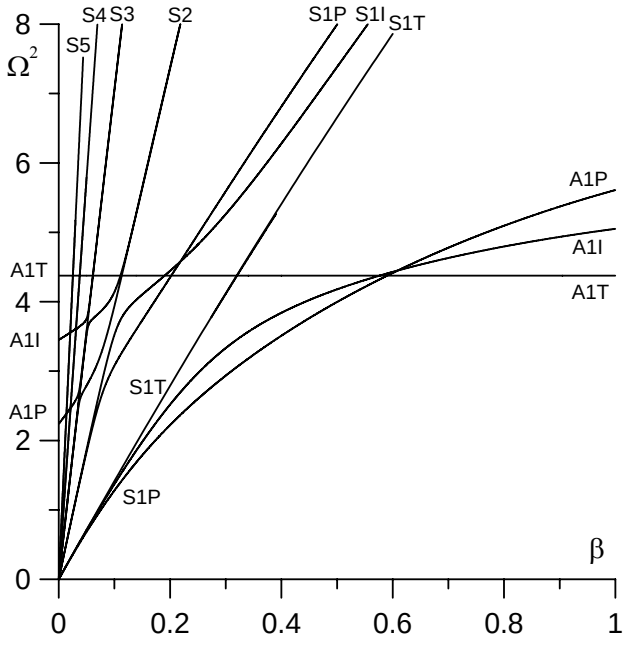

Fig. 2. Dependence of spectrum on beta and polarization for perfect conductivity (δ=0). Horizontal and near-horizontal lines correspond to Alfvén modes; lines running through the origin correspond to slow magnetosonic modes. Captions near the curve indicate a type of eigenmode ("A" – Alfvén mode, "S" – slow magnetosonic mode), the number of the eigenmode and the polarization of the eigenmode ("P" – poloidal (λ=0), "T" – toroidal ($\lambda\to\infty$), "I" – intermediate (λ=1); absent for higher-order slow magnetosonic modes due to a lack of space).

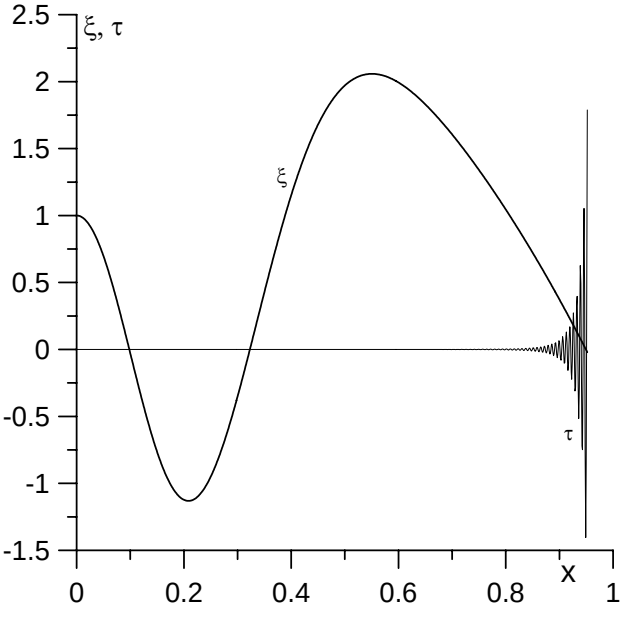

Fig. 3. Third order even eigenfunctions for α=10, β=0.01.

In the case of arbitrary polarization, eigenmode frequencies fill the area between poloidal and toroidal frequencies. This area is shaded in Fig. 1a. So, an external source with fixed frequency Ω can generate oscillations on certain magnetic shells, as predicted by Leonovich and Mazur (1998). Similarly, a given magnetic shell L=const can resonate with external sources if their frequencies fall in a certain fixed interval of frequencies, as was pointed out by Mager and Klimushkin (2002). It also means that the observed discrete spectrum will actually be a band-pass spectrum.

The physical frequency of the first Alfvén mode appears to be about 0.1–1 Hz, depending on L; and the physical frequency of the first magnetosonic mode is about 1 mHz.

Except for eigenmode spectra, we also investigated eigenfunctions. Numerical analysis has shown that transversal amplitudes ξ and η have no peculiarities, but longitudinal amplitude τ has an interesting behavior near the boundary. When a value $F=2\beta^{-1/2}\Omega$ is low, this behavior exposes itself in the form of a large single peak, and when this value is high, a single peak transforms into a series of positive and negative peaks, which become larger when moving to the boundary (Fig. 3). This was verified for several points with the same value of F. This effect is strongest at high values of the McIlwain parameter when a value $\varepsilon=1-x$ becomes a small parameter. In this case we can decompose Eq. (1) into a series of ε. As a result, we obtain one of the classical forms of the Bessel equation: $\varepsilon^2\tau''-9\varepsilon\tau'+\left(12+\varepsilon^2F^2\right)\tau=\frac{1}{4}\left(\xi'-\xi/\varepsilon\right)$. Its solution has the form $\tau=\tau_1+\tau_2$ with

$$\tau_1 = C\varepsilon^{-4}\left(Y_2\left(F\varepsilon\right) - AJ_2\left(F\varepsilon\right)\right), \tag{10}$$

$$\tau_2 = \tfrac{\pi}{8}\varepsilon^{-4}\left[Y_2\left(F\varepsilon\right)\int_{\varepsilon_0}^{\varepsilon}\zeta^4\left(\zeta\xi'+\xi\right)J_2\left(F\zeta\right)d\zeta - J_2\left(F\varepsilon\right)\int_{\varepsilon_0}^{\varepsilon}\zeta^4\left(\zeta\xi'+\xi\right)Y_2\left(F\zeta\right)d\zeta\right], \tag{11}$$

where J_2 and Y_2 are second order Bessel functions of type one and two correspondingly, C and A are constants, $\varepsilon_0=1-x_0$, ζ is the integration variable, corresponding to ε. In most cases $\tau_1\gg\tau_2$. Then we can drop the τ_2 term and the constant A is determined from boundary conditions (7) at $x=x_0$ ($\varepsilon=\varepsilon_0$): $A=Y_2\left(F\varepsilon_0\right)/J_2\left(F\varepsilon_0\right)$. If we change α from 10 to 1, function ξ won't change, and function τ will change its amplitude by 5 times. In any case, these functions perfectly fit the approximation (10); therefore, coefficient C significantly depends on α for both the single peak and the series of peaks.

Using the obtained result, we can determine the position $x_{\max}$ of the main peak of τ. To do this we differentiate Eq. (10) and equate the derivative to zero at $x=x_{\max}$. This gives us the value of $x_{\max}$ in dependence from x_0 and F. Choosing the values of F, corresponding to diagonal spectral lines, we determine the value of $x_{\max}$ for magnetic shells

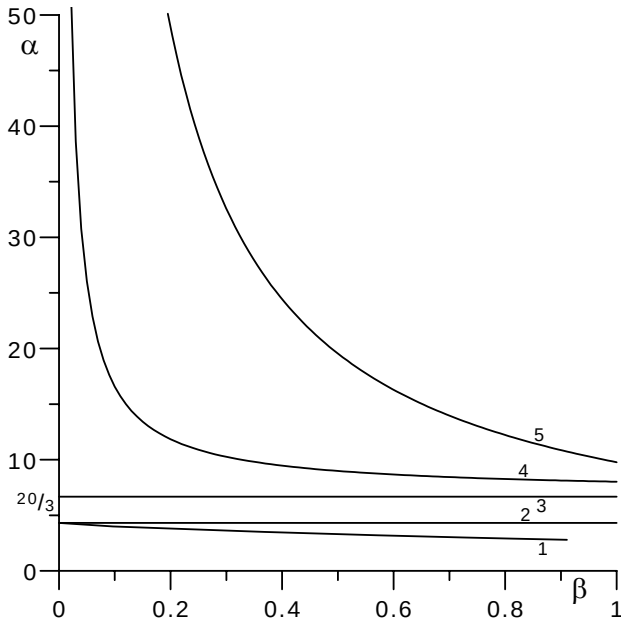

Fig. 4. Stability thresholds of the magnetospheric MHD modes: Flute modes (1 – nonlinear criterion (19), 2 – linear criterion (16), 3 – Gold criterion); Ballooning modes (4 – ballooning modes with ideally conductive ionosphere, 5 – ballooning modes with resistive ionosphere). The region of stability lies below the corresponding boundary.

with McIlwain numbers 2...10. They lie in a narrow altitude range, where plasma with a tied magnetic field experiences strong longitudinal oscillations with different frequencies simultaneously. As a result, one should expect the development of nonlinear effects and structures, leading to the excitation of higher-order harmonics. This effect should be especially strong in high magnetic latitudes and can be connected with nonlinear effects. Similar effects were observed by Freja (Stasiewicz et al., 1997) at the altitude 1475 km at $L\sim6$, which falls in the said range.

This extraordinary behavior of τ affects ξ negligibly, because all terms with τ in Eq. (1) contain a coefficient c^7, which is extremely small near the boundary.

4 Resistive boundary

In this case ($0<\delta<\infty$) boundary conditions (5), (6) are complex, and so are the solutions, i.e. dimensionless variables ξ, η, τ, and Ω. However, one should remember that dimensionless variables are related to actual physical quantities with complex relations. For example, to obtain the actual displacement one should multiply the dimensionless variables τ and ξ by $\exp\left(-ift+i\chi/\varepsilon\right)$, where χ/ε is a transversal eikonal; see Cheremnykh et al. (2004); Cheremnykh and Parnowski (2006b), and take a real part of the result. In particular, a solution $\xi\exp\left(-ift+i\chi/\varepsilon\right)$ gives a real function in the form

$$Re\left(\xi\exp\left(-ift+i\chi/\varepsilon\right)\right)=|\xi|\left|\exp i\chi/\varepsilon\right|$$

$$\exp\left(-\Gamma\omega_A t\right)\cos\left(\omega\omega_A t-\arg\xi-\arg\ \left(\exp i\chi/\varepsilon\right)\right).$$

Thus, the role of the dimensionless amplitude is held by $|\xi|$, and $\arg\xi$ describes the phase shift between oscillations in different parts of the field line. Because the cosine is an even function, each actual real solution corresponds with two dimensionless complex solutions with different signs of frequency and complex conjugate displacements. We shall give only solutions with positive values of the frequency.

In this section, we consider primarily poloidal perturbations, because the dependence of spectra on polarization is nearly the same at any conductivity.

4.1 Aperiodic perturbations

Although the boundary condition (5) is complex, there is one important case when it becomes real. It is the case of aperiodic perturbations when $\omega\equiv Re\,\Omega=0$, $\Omega=i\Gamma$, i.e. the complex frequency is purely imaginary and its imaginary part Γ will be called the growth rate for both positive and negative values. In the latter case it equals the decay rate with a negative sign. This class of solutions consists of flute (even) and incompressible (odd) perturbations. Equations (2), (4), (6) hold, and Eqs. (1), (3), (5) can be rewritten as

$$-\Gamma^2c^6b^{-1}\xi+\left(b^{-1}\xi'\right)'+4c^4b^{-2}\left(T_0+\alpha\beta\gamma^{-1}\xi\right)=0, \quad (12)$$

$$-\Gamma^2c^3\tau+T_0'=0, \quad (13)$$

$$\Gamma b\xi+\delta\left[2x\xi'-c^5\left(T_0+\alpha\beta\gamma^{-1}\xi\right)\right]\Big|_{x=\pm x_0}=0. \quad (14)$$

We analyze the set (12–14) to determine the dependence of the growth rate on parameters α, β, δ, and L. As before, we also investigated eigenfunctions. Before going to numerical results we shall give some analytical relations.

Let us consider the behaviour of the equations at low values of β. When Γ and β are small, Eq. (12) has two obvious solutions: ξ=const (flute modes) and ξ=const$\cdot(x+x^3)$ (incompressible modes). We shall assume that these constants equal one.

Even modes have solutions with $\Gamma=k\beta$, k=const. For them $\xi=1+\beta f\,(x)$. From the first order in β of Eqs. (12), (14) we obtain

$$k=\delta\left(\alpha\gamma^{-1}R_1-R_2\right),$$

$$f'=b\int_0^x\left(16c^5b^{-4}-4c^4b^{-2}\alpha\gamma^{-1}\right)dx, \quad (15)$$

where $R_1=8x_0\int_0^{x_0} c^4b^{-2}dx$, $R_2=32x_0\int_0^{x_0} c^5b^{-4}dx$. From Eq. (15) we see that $k\sim\delta$ and k grows when α increases and crosses zero at

$$\alpha\gamma^{-1} = R_2/R_1, \tag{16}$$

which corresponds to the stability threshold (2 in Fig. 4). Note that substituting the integrals in R_1 and R_2 with 1, we obtain the classical criterion of an interchange stability, obtained by Gold (1959) (3 in Fig. 4). However, integrals R_1 and R_2 depend on x_0 and thus from the McIlwain parameter L. At high values of L this dependence is very weak, though. The values of R_1 and R_2 in dependence on L are given in Table 1.

For odd modes $\xi=x+x^3+O(\beta)$. Casting this into Eq. (14), we obtain $\Gamma\left(1+x_0^2\right)+2\delta=0$, which is impossible when $\Gamma\to0$ at $\beta\to0$. Thus, odd modes cannot run through the origin of the growth rate plot ($\Gamma=0$, $\beta=0$). Nevertheless, it is possible when Γ tends to a finite value $\Gamma_0\neq0$ at $\beta\to0$. Zeroeth order in β of Eqs. (12), (14) gives us $\left(b^{-1}\xi'\right)'=\Gamma_0^2c^6b^{-1}\xi$, $\delta=-\frac{1}{2}b_0x_0^{-1}\Gamma_0\xi(x_0)/\xi'(x_0)$.

For even modes $\xi'(0)=0$, for odd ones $\xi(0)=0$. The latter equation can be easily solved numerically for fixed values of Γ_0. The odd curve tends to zero at $\delta=0$ and has a solution at any δ. For even modes there is a minimal value $\delta=\delta_0$, below which a solution ($\Gamma=\Gamma_0$, $\beta=0$) is absent. The values of δ_0, depending on L, are given in Table 1. In any case Γ_0 is negative, which corresponds to stability.

Now let us consider the behaviour of Eqs. (12–14) near the stability threshold, i.e. at $\Gamma\to0$. From Eq. (13) it is seen that $T_0\to$const. For even modes $\xi\approx1+\Gamma^np(x)$, $T_0\approx-\alpha\beta\gamma^{-1}+\Gamma^kq(x)$. At that Eq. (13) takes the form $\Gamma^2c^3\tau=\Gamma^kq'(x)$, which immediately gives us $k=2$. Taking this into account, Eq. (14) transforms into

$$\Gamma b_0+\delta\left(2x_0\Gamma^np'(x_0)-c_0^5\left(\Gamma^2q(x_0)+\alpha\beta\gamma^{-1}\Gamma^np(x_0)\right)\right)=0, \tag{17}$$

whence $n=1$. Now we can determine the form of τ near the stability threshold. For this purpose let us write the expression for T_0 in the zeroeth order in Γ: $c^{-3}\left(c^6b^{-1}\tau\right)'=4cb^{-2}-\alpha\gamma^{-1}$, whence taking into account Eq. (5),

$$\tau=bc^{-6}\left(\int_{x_0}^{x}\left(4c^4b^{-2}-\alpha\gamma^{-1}c^3-\alpha\beta\gamma^{-1}c^9b^{-1}\right)dx-\tfrac{1}{2}c_0^5x_0^{-1}b_0^{-1}\right). \tag{18}$$

The condition $\tau(0)=0$ gives us the expression for the stability threshold

$$\frac{\alpha}{\gamma}=\frac{\int_0^{x_0}4c^4b^{-2}dx+\frac{1}{2}c_0^5x_0^{-1}b_0^{-1}}{\int_0^{x_0}c^3dx+\beta\int_0^{x_0}c^9b^{-1}dx}=\frac{R_3(L)}{1+\beta R_4(L)}. \tag{19}$$

The values of R_3 and R_4 are presented in Table 1. To obtain the function τ for fixed β and L one should calculate α by the formula (19) and cast it into Eq. (17).

Table 1. Values of coefficients.

L	δ_0	R_1	R_2	R_3	R_4	R_5
2	2.555	1.632	5.028	2.602	0.515	5.759
3	2.522	1.887	5.806	2.541	0.506	5.853
4	2.495	2.002	6.159	2.533	0.504	5.861
5	2.478	2.068	6.361	2.531	0.504	5.863
6	2.465	2.111	6.492	2.530	0.504	5.863
7	2.456	2.141	6.584	2.530	0.504	5.863
8	2.450	2.163	6.652	2.530	0.504	5.863
9	2.444	2.180	6.705	2.530	0.504	5.863
10	2.440	2.194	6.746	2.530	0.504	5.863

It is easy to see from Eqs. (1–6) that Eq. (19) holds for the insulating boundary ($\Sigma_P=0$, $\delta\to\infty$), as well. For this reason the stability threshold in cases $0<\Sigma_P<\infty$ and $\Sigma_P=0$ will be the same. This result conforms to Theorem 2 from the paper by Hameiri (1999), which states that "a ballooning perturbation occurs for resistive bounding ends if, and only if, it occurs when bounding ends are insulators".

It is also interesting to determine the deviations of ξ from the constant, given by function $p(x)$. It satisfies in the first order in β Eq. (12) $\left(b^{-1}p'\right)'+4\alpha\beta\gamma^{-1}c^4b^{-2}p=0$ with given boundary conditions. They are $p'(0)=0$ and the condition following in the first order in β from Eq. (17) $2x_0p'(x_0)=\alpha\beta\gamma^{-1}c_0^5p(x_0)-b_0\delta^{-1}$. Its solution has the form $p(x)=\delta^{-1}F(x)$. Thus,

$$\xi = 1+\Gamma\delta^{-1}F(x).$$

In particular, this means that at $\delta\to\infty$ ($\Sigma_P=0$) $\xi=$const, and at $\delta=0$ ($\Sigma_P\to\infty$) the deviations become infinite, i.e. flute modes cannot exist.

For odd functions $T_0=0$. This is seen from the symmetry and can be proven in the following way. Let us introduce $u(x)=\xi(x)/\xi(x_0)$, $A=T_0/\xi(x_0)$, $t(x)=\tau(x)/\xi(x_0)$. From Eqs. (4), (10) one can easily obtain

$$t=bc^{-6}\left(-\tfrac{1}{2}c_0^5x_0^{-1}b_0^{-1}+\int_{x_0}^{x}\left(4c^4b^{-2}u+Ac^3\left(\beta^{-1}+c^6b^{-1}\right)\right)dx\right). \tag{20}$$

The condition $t'(0)=0$ can hold only when $A=0$. This result is also quite obvious from physical speculations: $T_0=\gamma p\,\mathrm{div}\boldsymbol{\xi}$ determines the compressibility of perturbations and the condition $T_0=0$ corresponds to incompressible perturbations. Equation (12) acquires the form

$$\left(b^{-1}u'\right)'+4c^4b^{-2}\alpha\beta\gamma^{-1}u=0. \tag{21}$$

It has boundary conditions $u(0)=0$, $u(x_0)=1$, $u'(x_0)=\frac{1}{2}c_0^5x_0^{-1}\alpha\beta\gamma^{-1}$. This is possible only with a certain product

$$\alpha\beta\gamma^{-1} = R_5(L). \tag{22}$$

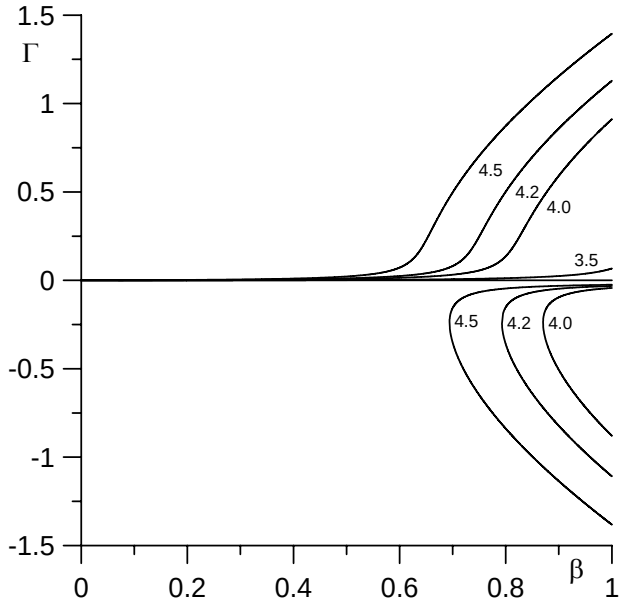

Fig. 5a. Spectrum of flute modes for δ=0.01 (local noon).

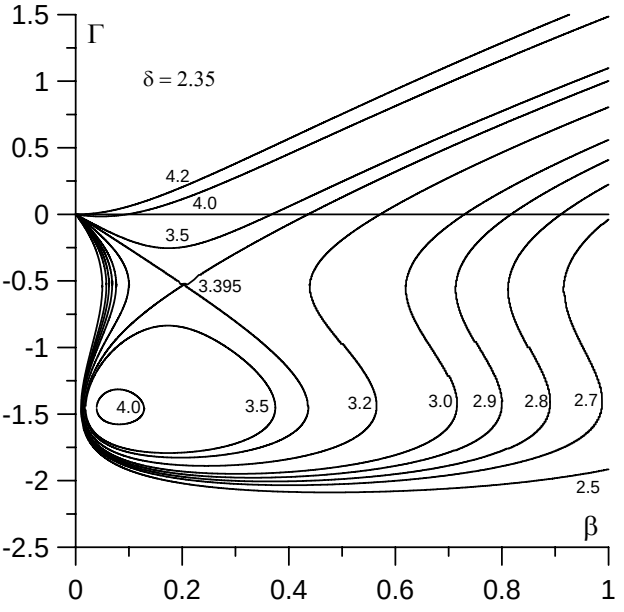

Fig. 5c. The same for δ=2.35 (slightly below the δ_0 value).

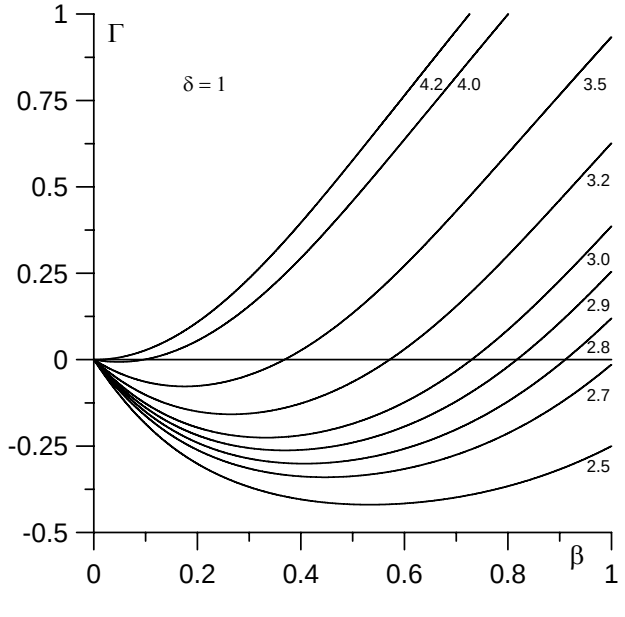

Fig. 5b. The same for δ=1 (dawn/dusk).

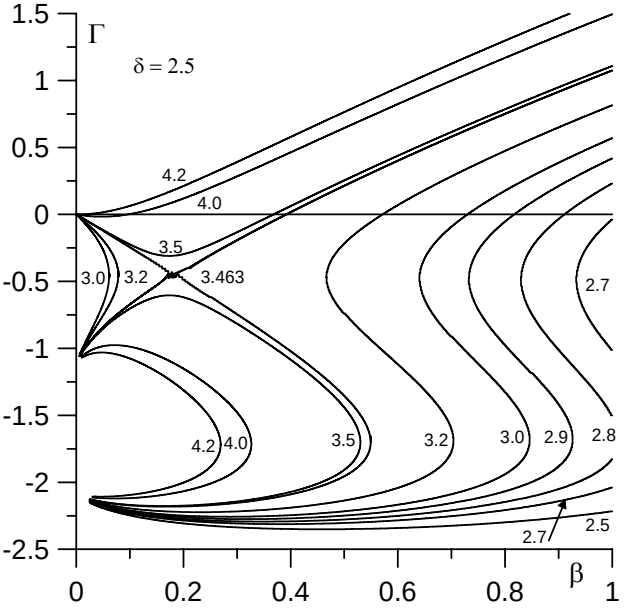

Fig. 5d. The same for δ=2.5 (slightly above the δ_0 value).

Its values are listed in Table 1. With a given value of $\alpha\beta\gamma^{-1}$ we can calculate $u\,(x)$ by Eq. (21) and casting into Eq. (20) obtain $t\,(x)$.

It can be seen from Table 1 that at $\beta<1$ the values of α corresponding to the stability threshold for flute perturbations are much lower than for the incompressible perturbations.

Let us go to the numerical results. They are presented on Figs. 5a–e in the form of $\Gamma\,(\beta)$ plots at constant values of α and δ. We have chosen the somewhat unrealistic value L=10 to emphasize some effects, which are nearly unnoticeable at low L values. We considered odd and even modes separately. Special attention was paid to values δ=10^{-2}, 1, 10^2, which correspond to day, dawn/dusk, and night sectors. For even modes we also considered values δ=2.35 and δ=2.5, which fall slightly above and below δ_0.

The corresponding dependences are shown in Fig. 5. For odd modes, similar plots have no interesting features. In all cases the intersections with the β axis are described by Eq. (19) for even modes and Eq. (22) for odd ones. For the

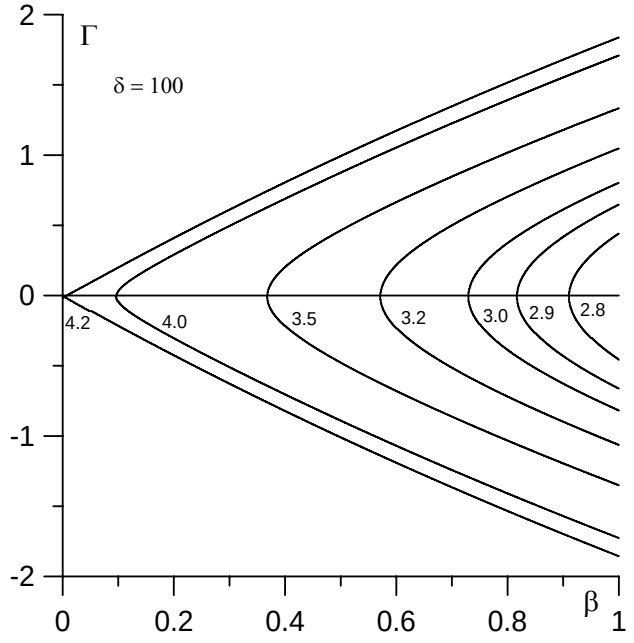

Fig. 5e. The same for δ=100 (local midnight).

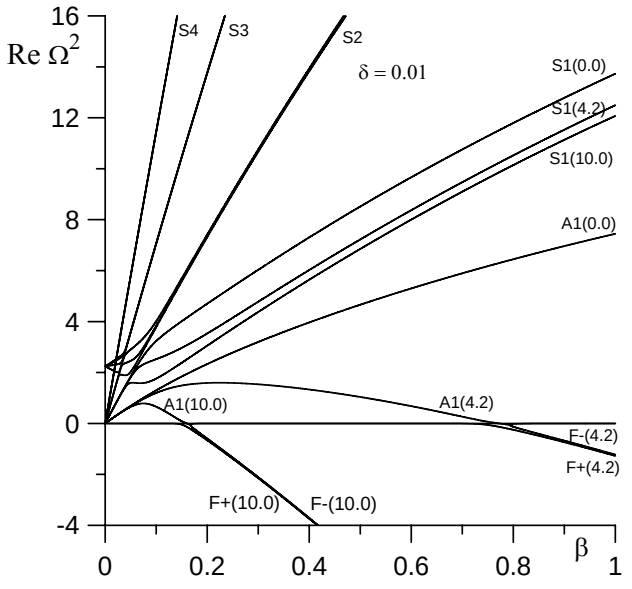

Fig. 6. Dependence of spectrum on beta and profile of pressure for δ=0.01. Captions near the curve indicate the type of eigenmode ("A" – Alfvén mode, "S" – slow magnetosonic mode, "F" – flute mode), number of eigenmode for periodic modes or growth rate sign for aperiodic modes and value of α in parentheses.

curves running through origin, Eq. (18) also holds true. The values of Γ_0 differ slightly from those given in Table 1, which can be caused by a dropped term with τ.

We also investigated the eigenfunctions. Near the stability threshold, both even and odd functions completely coincide with the above-mentioned analytical predictions. In the general case, far from the stability threshold, it is possible to obtain an approximate expression for τ when $x\sim1$. This is possible only for large McIlwain numbers. Function τ in this case can be expressed in the form $\tau=\tau_1+\tau_2+\tau_3$, where

$$\tau_1 = R\varepsilon^{-4}\left(K_2(G\varepsilon) - AI_2(G\varepsilon)\right),$$

$$\tau_2 = -\tfrac{1}{4}\varepsilon^{-4}\varepsilon_0^3\xi(x_0)\, I_2(G\varepsilon)\big/ I_2(G\varepsilon_0),$$

$$\tau_3 = \tfrac{1}{4}\varepsilon^{-4}\left[K_2(G\varepsilon)\int_{\varepsilon_0}^{\varepsilon}\zeta^4\left(\zeta d\xi\big/d\zeta+\xi\right)I_2(G\zeta)\,d\zeta - I_2(G\varepsilon)\int_{\varepsilon_0}^{\varepsilon}\zeta^4\left(\zeta d\xi\big/d\zeta+\xi\right)K_2(G\zeta)\,d\zeta\right].$$

Here I_2, K_2 are modified second order Bessel functions of type one and three, correspondingly, $A=K_2(G\varepsilon_0)\big/I_2(G\varepsilon_0)$, $G=2\beta^{1/2}\Gamma$. Functions τ_1 and τ_3 vanish at $x=x_0$, and function τ_2 ensures the satisfaction of boundary condition (5). Boundary condition (6) can be satisfied by scaling the coefficient R in τ_1. Term τ_3 influences τ weakly.

4.2 Periodic perturbations

Numerical calculations show that ω and Γ significantly depend on δ. At low values of δ the dependence of $Re\Omega^2=\omega^2-\Gamma^2$ on β for periodic perturbations, shown in Fig. 6, is very similar to the dependence of Ω^2 on β at δ=0, shown in Fig. 2. Note that at fixed parameters the eigenmode spectrum is discrete. It contains harmonics with both zero and non-zero frequencies. The spectrum in this case consists of curves describing Alfvén and slow magnetosonic modes, which intersect at $\lambda=\infty$, and couple at finite values of λ.

Numerical calculations demonstrate that the inclination of the spectral lines in the (ω, β) plane does not depend on δ. This effect can be explained in the following way. In Fig. 6 one can see that slow magnetosonic modes at low β are straight lines $\Omega^2=p\beta$. It follows from Eq. (6) that $Re p$ does not depend on δ and $Re p \gg Im p$, because $|\omega|\gg|\Gamma|$ for periodic perturbations. Earlier we mentioned that in the conductive boundary case longitudinal displacement τ is larger than transversal displacement ξ by several orders. Numerical calculations show that this property holds for boundary conditions (5), (6) as well. Considering this, let us find the values of $Re p$ for even modes. Note that odd frequencies are higher and thus are less interesting. Dropping terms $\sim\xi$ in Eq. (3), we obtain an equation for τ for even modes: $\left(c^{-3}\left(c^6 b^{-1}\tau\right)'\right)'+p\tau c^3=0$. It follows from this equation that $Re p$ does not depend on polarization. Numerical solutions of the eigenvalue problem give us discrete values $p(L)$ for different even harmonics of slow magnetosonic modes. For L=10 they equal: for the first harmonics 14.6, for the second – 38.2, for the third – 72.3. Taking into account that for L=10 $\tau/\xi>\sim10^3$, for realistic conductivity the main

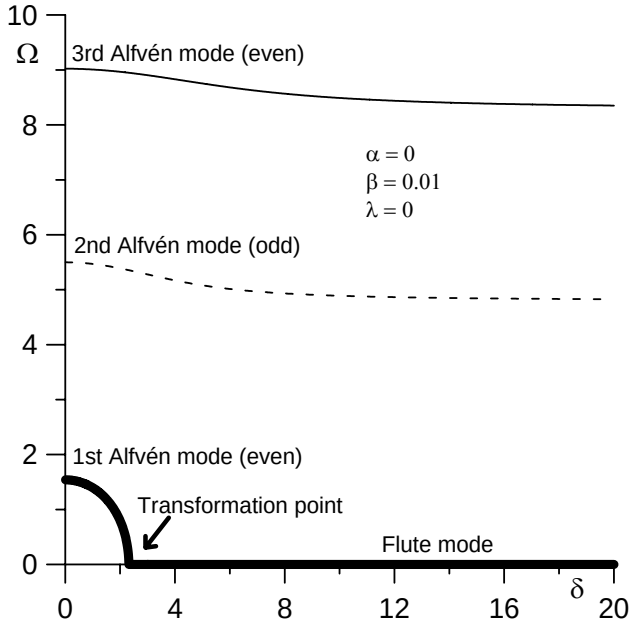

Fig. 7. Dependence of spectrum on ionospheric conductivity for β=0.01. The first Alfvén mode exists only at δ<2.35 (in day sector).

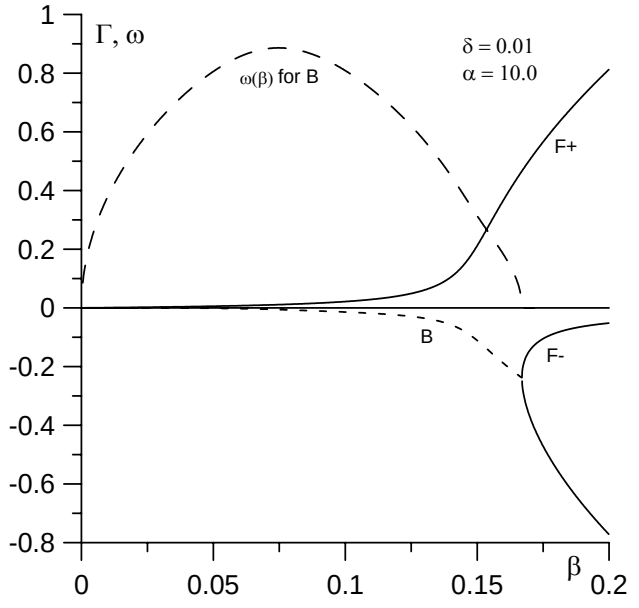

Fig. 8a. Growth rate spectrum for δ=0.01 (local noon). Note that the F+ mode becomes unstable right before the ballooning mode B splits into two F− modes.

terms in Eq. (5) are proportional to δ, thus this condition in main terms does not depend on δ.

At small values of β Alfvén frequencies do not depend on α, but depend on δ. For harmonics of second order and higher these frequencies decrease with the growth of δ (for second even mode from ω=9 at $\delta\leq$1 to ω=8.3 at $\delta\geq$100; growth rate Γ is negative and its absolute value does not exceed 0.002). The frequency of the first mode quickly decreases, reaching zero at $\delta\sim$2.3 for β=0.01, then it disappears (Fig. 7). This means that this mode can be observed only in the day sector. At low β values, the inclination of the Alfvén spectral lines is determined by α in the same way as for conductive boundary.

At ω=0 this mode laces with aperiodic flute modes. The lacing point contains a bifurcation: rightwards from this point there are two F− flute modes. This effect is not visible clearly enough in Fig. 6, so we present it in detail in Fig. 8a. Figures 8a–c show a dependence of the growth rate Γ from β. Leftwards from the lacing point, there is a coupling of Alfvén mode B with flute mode F+, which determines the stability threshold. Thus, rightwards from the lacing point the growth rate of the F+ mode rapidly increases.

In the previous section, we considered the behaviour of flute modes F+ and F−. In particular, the calculations show that for low δ mode F+ becomes unstable when β exceeds a certain value, which depends on α. However, at low δ the growth rate of mode F+ between the mentioned point and the coupling point is so small that the characteristic development time of instability exceeds the characteristic variation time

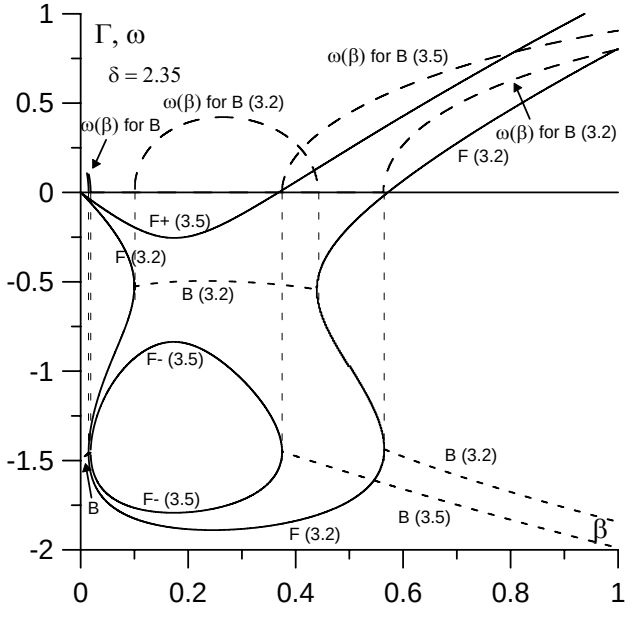

Fig. 8b. Growth rate spectrum for δ=2.35 (dawn/dusk). Note that flute modes F+ (3.5) and F (3.2) become unstable exactly when the ballooning modes B (3.5) and B (3.2) split.

of the equilibrium processes. For this reason, we should consider the coupling point to be the practical stability threshold.

Calculations show that growth of δ essentially changes the coupling of Alfvén and slow magnetosonic modes. Figure 9 shows the plots of the coupling point for different values of

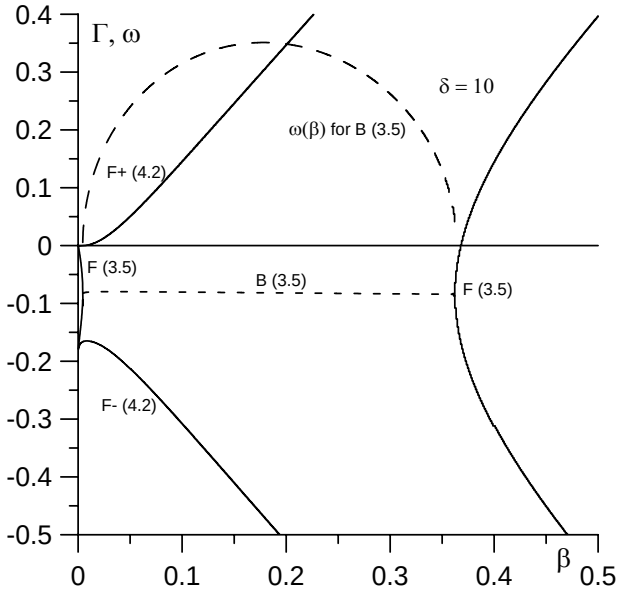

Fig. 8c. Growth rate spectrum for δ=10 (local midnight). Flute mode F (3.5) becomes unstable right after ballooning mode B splits. Flute mode F+ (4.2) is always unstable.

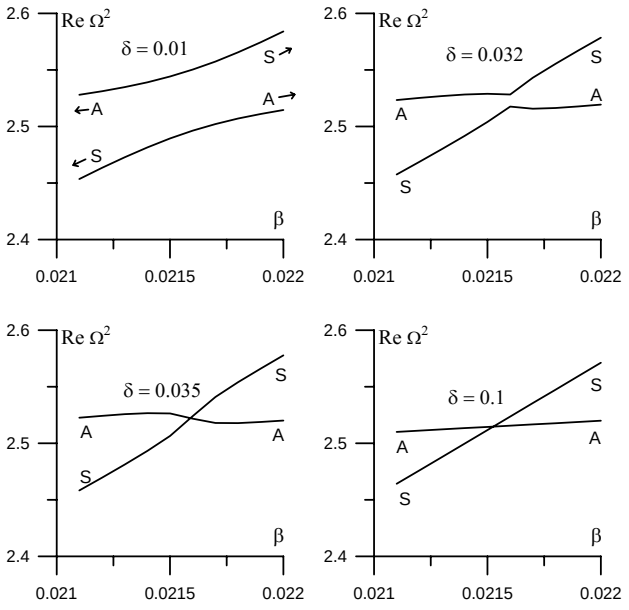

Fig. 9. Alfvén-magnetosonic coupling for different ionospheric conductivities. At high conductivity these modes "couple" and at low conductivity they intersect. "A" – Alfvén mode, "S" – slow magnetosonic mode.

δ. It is seen that at δ=0.01 coupling is usual. When δ grows the spectral lines deform and tend closer. Finally, at large δ coupling transforms into intersection. This means that energy transfer between "high"- and "low"-frequency oscillations disappears.

The behaviour of Alfvén modes is closely related to the behaviour of aperiodic perturbations. In the region of the disappearance of the first even mode, i.e. at $\delta\sim 2\div 3$, aperiodic flute modes show complicated behaviour in the (Γ, β) plane, featuring closed circles and S-shaped arcs. Calculations show that at every point of these plots, where $\partial\Gamma/\partial\beta$ tends to infinity, the aperiodic mode laces with the periodic mode. At that point, the periodic mode is directed by the outward normal to the aperiodic mode. Examples of such behaviour are shown in Fig. 8b. In the same figure the frequencies ω of Alfvén modes are also plotted. One can see that the growth rates are considerably negative. When δ grows further, the lacing of the Alfvén and flute modes features a bifurcation, but the growth rates are much lesser.

At large δ values $|\Gamma|\sim\delta^{-1}$. An example of such behaviour is shown in Fig. 8c. At low δ values $|\Gamma|\sim\delta$. Thus, perturbations develop in the day and night sectors, and decay in dawn and dusk sectors.

In Figs. 8a–c one can see an important feature: when the flute growth rate becomes positive and significant in value, an Alfvén-ballooning mode with non-zero frequency disappears or reappears. Thus, it is possible to discover a flute instability (which is aperiodic and is very hard to be discovered directly) by monitoring the frequency of the first Alfvén mode. When this frequency becomes small, it indicates that flute instability is about to develop.

5 On the influence of nonlinear terms in pressure

Now let us discuss the accuracy of the obtained results. In our earlier papers (Cheremnykh et al., 2004; Cheremnykh and Parnowski, 2006b), we pointed out that the accuracy of the equations of small oscillations should not exceed the accuracy of the equation of equilibrium, which was linear in β. Thus, we should have replaced the coefficient $\left(c^6b^{-1}+\beta^{-1}\right)^{-1}$ in Eq. (4) with β, thus dropping the nonlinear term in β. From the physical point of view this means that we neglect the plasma pressure in comparison with magnetic pressure. Nevertheless, we see that when β is not very small, this correction is significant in the equatorial region, where $c^6b^{-1}\sim 1$. Thus, all of the given above results were obtained with this correction. To estimate its influence we additionally calculated flute eigenmode spectra without it (incompressible modes are not affected by it, because T_0=0 for them). The most prominent difference is the flute stability threshold (1 in Fig. 4). The threshold Eq. (19) with correction appears lower than the threshold without correction. These facts indicate the importance of taking into account nonlinear terms in β.

6 Conclusion

Using both numerical and analytical methods, we analyzed the eigenmode spectra and eigenfunctions for ballooning perturbations in a dipole model of the inner magnetosphere of

the Earth for a conductive and resistive boundary. In the latter case, perturbations are divided into periodic and aperiodic ones (having zero frequency). The main results are:

1. The eigenmode spectrum is discrete and equidistant and consists of Alfvén (transversal) and slow magnetosonic (longitudinal) modes, which couple due to a field line curvature, plasma pressure and plasma compressibility. The frequencies of the first eigenmodes of each type are $\sim$1 Hz for Alfvén modes and $\sim$1 mHz for slow magnetosonic modes. In the case of a resistive boundary, there are also flute and incompressible modes with zero frequency.

2. Alfvén and slow magnetosonic modes decay in dawn and dusk sectors of the magnetosphere much stronger than in day or night sectors. This means that the Pc pulsations' spectrum should be more intense in day and night sectors than in dawn and dusk sectors.

3. MHD stability is defined by flute modes. The corresponding stability criterion (19) was derived. Slow magnetosonic modes are always stable. Flute instability is accompanied by the disappearance or reappearance of the Alfvén-ballooning mode with non-zero frequency, which can be used for diagnostic purposes.

4. Alfvén and flute modes can mutually transfer into each other. This phenomenon can strongly affect plasma stability.

5. Longitudinal displacements have a large peak near the boundary, which can cause the development of nonlinear structures. The position of the peak is determined and can be associated with nonlinear structures observed by Freja. Transversal displacements of flute perturbations deviate from the constant along the field line due to the field line curvature. The value of the deviations is calculated.

6. An influence of nonlinear terms in pressure was estimated. They affect both the stability and spectra of the perturbations. Incompressible modes are unaffected, since the nonlinear term appears in term (4), which vanishes in this case.

Now let us mention possible observational manifestations of results listed above. Observed spectrum should be a bandpass spectrum, with Alfvén modes of about 1 Hz and slow magnetosonic modes of about 1 mHz. The overall spectral power in the day and night sectors should be larger than in the dawn and dusk ones. Flute instability can be detected by observing extremely low-frequency oscillations; appearance or disappearance of such modes indicates that flute instability is about to develop. The first Alfvén mode can be observed only in the day sector. At altitudes about 1500 km at L=6 there are small-scale structures with large amplitudes (confirmed by Freja observations).

Acknowledgements. Topical Editor I. A. Daglis thanks two anonymous referees for their help in evaluating this paper.

References

Chan, A. A., Xia, M., and Chen, L.: Anisotropic Alfvén-ballooning modes in Earth's magnetosphere, J. Geophys. Res., 99(A9), 17 351–17 366, 1994.

Cheng, A. F.: Magnetospheric interchange stability, J. Geophys. Res., 80(A10), 9900–9904, 1985.

Cheng, C. Z., Chang, T. C., Lin, C. A., and Tsai, W. H.: Magnetohydrodynamic theory of field line resonances in the magnetosphere, J. Geophys. Res., 98(A7), 11 339–11 347, 1993.

Cheremnykh, O. K. and Parnowski, A. S.: The theory of ballooning perturbations in the inner magnetosphere of the Earth, Adv. Space Res., 33(5), 769–773, 2004.

Cheremnykh, O. K. and Parnowski, A. S.: Influence of ionospheric conductivity on the ballooning modes in the inner magnetosphere of the Earth, Adv. Space Res., 37(3), 599–603, 2006a.

Cheremnykh, O. K. and Parnowski, A. S.: Flute and Ballooning Modes in the Inner Magnetosphere of the Earth: Stability and Influence of the Ionospheric Conductivity, in: Space Science: New Research, edited by: Maravell, N. S., 71–108, Nova Science Publishers, New York, 2006b.

Cheremnykh, O. K., Parnowski, A. S., and Burdo, O. S.: Ballooning modes in the inner magnetosphere of the Earth, Planet. Space Sci., 52(13), 1217–1229, 2004.

DeMichelis, P., Daglis, I. A., and Consolini, G.: An average image of proton plasma pressure and of current systems in the equatorial plane derived from AMPTE/CCE-CHEM measurements, J. Geophys. Res., 104(A12), 28 615–28 624, 1999.

Dewar, R. L. and Glasser, A. H.: Ballooning mode spectrum in general toroidal system, Phys. Fluids, 26(10), 3038–3052, 1983.

Elsasser, W. M.: Induction Effects in Terrestrial Magnetism Part I. Theory, Phys. Rev. B, 69(3–4), 106–116, 1946.

Gold, T.: Motions in the magnetosphere of the Earth, J. Geophys. Res., 64, 1219–1226, 1959.

Hameiri, E.: Ballooning modes on open magnetic field lines, Phys. Plasmas, 6(3), 674–685, 1999.

Hameiri, E. and Kivelson, M. G.: Magnetospheric Waves and the Atmosphere-Ionosphere Layer, J. Geophys. Res., 96(A12), 21 125–21 134, 1991.

Hameiri, E., Laurence, P., and Mond, M.: The ballooning instability in space plasmas, J. Geophys. Res., 96(A2), 1513–1518, 1991.

Klimushkin, D. Yu.: Spatial structure of transversally small-scale hydromagnetic waves in a plane finite-β model magnetosphere, Planet. Space Sci., 45(2), 269–279, 1997.

Lakhina, G. S., Mond, M., and Hameiri, E.: Ballooning Mode Instability at the Plasmapause, J. Geophys. Res., 95(A4), 4007–4016, 1990.

Leonovich, A. S. and Mazur, V. A.: Standing Alfvén waves with m$\gg$1 in an axisymmetrical magnetosphere excited by a stochastic source, Ann. Geophys., 16, 900–913, 1998, http://www.ann-geophys.net/16/900/1998/.

Liu, W. W.: A note on the interchange stability criterion, J. Geophys. Res., 101(A12), 27 443–27 447, 1996.

Lui, A. T. Y. and Hamilton, D. C.: Radial profile of quiet time magnetospheric parameters, J. Geophys. Res., 97(A12), 19 325–19 332, 1992.

Mager, P. N. and Klimushkin, D. Yu.: Theory of azimuthally small-scale Alfvén waves in an axisymmetric magnetosphere with small but finite plasma pressure, J. Geophys. Res., 107(A11), 1356, doi:10.1029/2001JA009137, 2002.

McIlwain, C. E.: Coordinates for mapping the distribution of geomagnetically trapped particles, J. Geophys. Res., 66(12), 3681–3691, 1961.

Rogers, B. and Sonnerup, B. U. O.: On the interchange instability, J. Geophys. Res., 91(A8), 8837–8845, 1986.

Southwood, D. J. and Kivelson, M. G.: Magnetospheric interchange motion, J. Geophys. Res., 94(A1), 299–308, 1989.

Stasiewicz, K., Gustafsson, G., Marklund, G., Lindqvist, P.-A., Clemmons, J., and Zanetti, L.: Cavity resonators and Alfvén resonance cones observed on Freja, J. Geophys. Res., 102(A2), 2565–2575, 1997.

Swift, D. W.: The possible relationship between the auroral breakup and the interchange instability of the ring current, Planet. Space Sci., 15(8), 1225–1237, 1967.